

Environmental Dependence of Cold Dark Matter Halo Formation

H.Y. Wang^{1,3,4*}, H.J. Mo^{2,3}, Y.P. Jing^{3,4}

¹*Center for Astrophysics, University of Science and Technology of China, Hefei, Anhui, China*

²*Department of Astronomy, University of Massachusetts, Amherst MA 01003-9305, USA*

³*Shanghai Astronomical Observatory; the Partner Group of MPA, Nandan Road 80, Shanghai 200030, China*

⁴*Joint Institute for Galaxy and Cosmology (JOINGC) of SHAO and USTC*

Accepted Received; in original form

ABSTRACT

We use a high-resolution N -body simulation to study how the formation of cold dark matter (CDM) halos is affected by their environments, and how such environmental effects produce the age-dependence of halo clustering observed in recent N -body simulations. We estimate, for each halo selected at redshift $z = 0$, an ‘initial’ mass M_i defined to be the mass enclosed by the largest sphere which contains the initial barycenter of the halo particles and within which the mean linear density is equal to the critical value for spherical collapse at $z = 0$. For halos of a given final mass, M_h , the ratio M_i/M_h has large scatter, and the scatter is larger for halos of lower final masses. Halos that form earlier on average have larger M_i/M_h , and so correspond to higher peaks in the initial density field than their final masses imply. Old halos are more strongly clustered than younger ones of the same mass because their initial masses are larger. The age-dependence of clustering for low-mass halos is entirely due to the difference in the initial/final mass ratio. Low-mass old halos are almost always located in the vicinity of big structures, and their old ages are largely due to the fact that their mass accretions are suppressed by the hot environments produced by the tidal fields of the larger structure. The age-dependence of clustering is weaker for more massive halos because the heating by large-scale tidal fields is less important.

Key words: dark matter - large-scale structure of the universe - galaxies: haloes - methods: statistical

1 INTRODUCTION

In the standard cold dark matter (CDM) paradigm of structure formation, virialized CDM halos are both the building blocks of the large-scale structure of the Universe and the hosts within which galaxies are supposed to form. During the last decade, the properties of CDM halos, such as their internal structure, formation histories and clustering properties, have been studied in great detail using both N -body numerical simulations and analytical models. These studies have shown that the halo bias depends strongly on halo mass, in the sense that more massive halos are more strongly clustered (e.g., Mo & White 1996; Jing 1998; Seljak & Warren 2004). This mass dependence of the halo bias has played a crucial role in understanding the correlation function of both dark matter and galaxies, via the halo model (e.g., Mo, Jing & Börner 1997; Ma & Fry 2000; Seljak 2000), the halo occupation models (e.g., Jing, Mo & Börner 1998; Peacock & Smith 2000; Zheng et al. 2005), and the conditional luminosity function (e.g., Yang, Mo & van den Bosch 2003).

Recently Gao et al (2005), using a very large N -body simulation of a Λ CDM cosmology, reexamined the dependence of halo bias on the properties of dark matter halos. They found that, for low-mass halos at redshift $z = 0$ with $M_h \ll M_\star$ ¹, the bias depends not only on the mass but also on the formation time of dark matter halos. For a given mass, halos that have earlier formation times are on average more strongly clustered in space. This age-dependence of halo clustering has been confirmed by a number of independent studies (e.g. Zhu et al. 2006; Harker et al. 2006). Since halo formation time is known to be correlated with halo concentration (e.g. Navarro, Frenk & White 1997; Jing 2000; Wechsler et al 2002; Zhao et al. 2003a,b; Lu et al. 2006), the age dependence of halo clustering also shows up as a halo-concentration dependence of halo clustering (Wechsler et al. 2005). For massive halos with $M_h \gg M_\star$, the age-dependence may be reversed, as shown in Wechsler et al. (2005) and Wetzel et al. (2006).

Although the mass-dependence of halo clustering is well understood in the excursion-set model based on spherical collapse in Gaussian initial density field (Mo & White 1996), the formation-time dependence (or age-dependence) is not. In the simplest excursion-set model from which the Press-Schechter formula is derived (Bond et al. 1991), the formation history of a halo is entirely determined by the local density field, independent of the mass

* E-mail: whywang@mail.ustc.edu.cn

¹ M_\star is the characteristic mass scale at which the RMS of the linear density field is equal to 1.686 at the present time. For the present simulation $M_\star \approx 1.0 \times 10^{13} h^{-1} M_\odot$.

distribution on larger scales. Therefore, the large-scale clustering of halos is independent of formation time in this model. An age-dependence of halo clustering is expected in the excursion-set model based on ellipsoidal collapse (Sheth, Mo & Tormen 2001), because here the collapse of a halo depends not only on the local density field but also on the tidal field generated by its large-scale environment. Unfortunately, this aspect of the model was not explored in any detail in Sheth et al. (2001). Instead, these authors used a mean relation between halo mass and the shape parameter of the large-scale tidal field to derive an average critical collapse overdensity that depends only on halo mass.

Since the properties of galaxies that form in a halo are expected to depend on the formation history of the halo, understanding the origin of the age-dependence of halo clustering is crucial for a better understanding about how galaxies are related to their large-scale environments. In this paper we use a high-resolution N -body simulation to study how the formation of dark matter halos is affected by their environments, and how such environmental effects can be used to understand the age-dependence of halo clustering. The outline of the paper is as follows. In Section 2 we describe briefly the simulation to be used and how dark halos are identified. In Section 3 we study the age-dependence of halo clustering in terms of halo properties in the initial density field. In Section 4 we examine the environments of dark halos and how they may affect the formation histories of dark matter halos. We discuss and summarize our results in Section 5.

2 SIMULATION AND DARK MATTER HALOS

The simulation used in this paper was obtained using the P³M code described in Jing & Suto (2002). This simulation assumes a spatially-flat Λ CDM model, with density parameters $\Omega_m = 0.3$ and $\Omega_\Lambda = 0.7$, and the cold dark matter power spectrum given by Bardeen et al (1986), with a shape parameter $\Gamma = \Omega_m h = 0.2$ and an amplitude specified by $\sigma_8 = 0.9$. The CDM density field was represented by 512^3 particles, each having a mass of $M_p \sim 6.2 \times 10^8 M_\odot$, in a cubic box of $100 h^{-1}$ Mpc. The softening length is $10 h^{-1}$ kpc. Outputs are made at 60 different redshifts between $z = 15$ and $z = 0$, with an interval given by $\Delta \ln(1 + z) = 0.047$.

Halos are identified with the friends-of-friends algorithm (e.g. Davis et al. 1985) with a linking length 0.2 times the mean particle separation. In order to ensure that only physically bound systems are selected, we discard all particles selected into a halo but are not bound on

the basis of their binding energies. However, this step does not have any significant impact on our results. Halos at $z = 0$ are related to their progenitors at higher z through halo merging trees. A halo in an earlier output is considered to be a progenitor of the halo in question if more than half of its particles are found in the final halo. The formation time of a halo is defined as the time when its most massive progenitor has exactly half of the final mass. Interpolations between adjacent outputs were adopted when estimating the formation times. In Fig. 1 we show the distribution of formation redshift for halos in two mass ranges. These results are similar to those obtained in Li et al. (2005).

3 THE AGE DEPENDENCE OF HALO CLUSTERING

In order to examine the age-dependence of halo clustering in the present simulation, we estimate the mean overdensity of dark matter within a sphere of a given radius R around each dark matter halo, $\delta_h(R) \equiv M(R)/\overline{M}(R) - 1$, where $M(R)$ is the mass within a radius R around the halo, and $\overline{M}(R) = (4\pi R^3/3)\overline{\rho}$ with $\overline{\rho}$ being the mean mass density of the universe. We estimate the bias parameter of a given set of halos using

$$b = \frac{\langle \delta_h(R) \rangle}{\langle \delta_m(R) \rangle}, \quad (1)$$

where $\langle \delta_h(R) \rangle$ is the average overdensity over the set of halos in consideration, and $\langle \delta_m(R) \rangle$ is the average overdensity within all spheres of radius R centered on dark matter particles. This definition of b is different from that in Gao et al. (2005) where the auto-correlation function of halos is used to derive the bias factor. Our test showed that these two definitions lead to similar results. The advantage of our definition is that the statistic is more stable owing to the fact that there are many more dark matter particles than halos in the simulation. Fig. 2 shows the bias parameter obtained in this way as a function of halo formation time for halos of different masses. Results shown are the average for five different choices of R : 5, 7.5, 10, 12.5 and $15 h^{-1}\text{Mpc}$. We see clearly that the bias factor increases with halo formation redshift for low-mass halos ($M_h < M_\star$) and the dependence becomes weaker for $M_h \sim M_\star$. These results are in good agreement with those obtained by Zhu et al. (2006), using the same set of simulations, from the auto-correlation functions of dark halos. For massive halos, there is indication that the age-dependence may be reversed. Unfortunately, the present simulation is too small to allow us to study the age-dependence in detail for massive halos with $M_h > 10^{13} h^{-1} M_\odot$. Note that part of the inverse relation between halo bias and formation time for massive halos is due to the use of non-zero mass bin. More

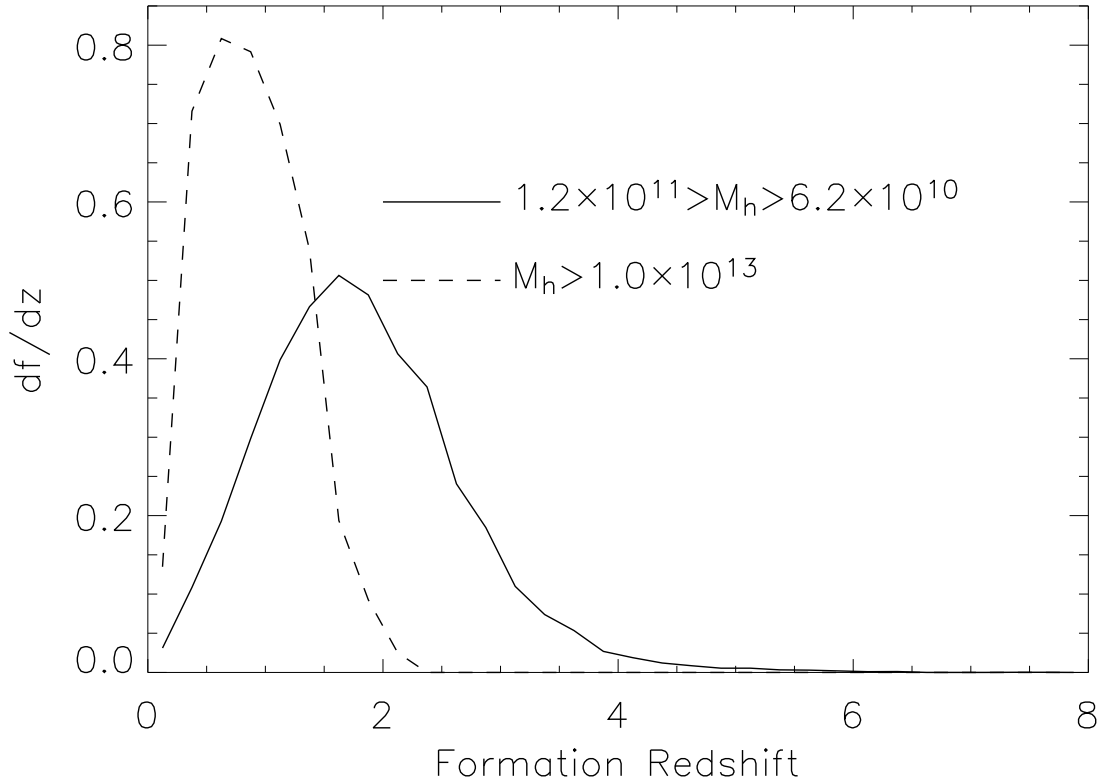


Figure 1. The distribution of formation redshift for halos in two mass ranges, $1.2 \times 10^{11} h^{-1} M_{\odot} > M_h > 6.2 \times 10^{10} h^{-1} M_{\odot}$ (solid curve) and $M_h > 1.0 \times 10^{13} h^{-1} M_{\odot}$ (dashed curve).

massive halos within such a bin have, on average, larger bias due to the strong mass-dependence of halo bias for massive halos. Since the more massive halos are on average also younger, an inverse relation between halo bias and formation time can be produced, even if age-dependence of halo bias is completely absent for massive halos of a given mass.

In order to understand the origin of the age-dependence of halo clustering, we examine the properties of dark matter halos in the initial density field. For each halo identified at the present time ($z = 0$), we trace the positions of all its particles back to the initial condition, and define the initial center of the halo to be the barycenter of these particles in the initial density field (set at $z_i = 72$). At each center, we find the largest spherical region within which the initial average overdensity exceeds the critical value δ_{sc} for spherical collapse at $z = 0$. We call this sphere the initial patch of the halo, and denote the mass within it by M_{i1} . For a given halo, its initial center may be contained in the initial patches of other halos, and we denote the mass within the largest patch by M_i . By definition $M_{i1} \leq M_i$. According to Press-Schechter theory (Press & Schechter 1974), the mass of the halo in which the center

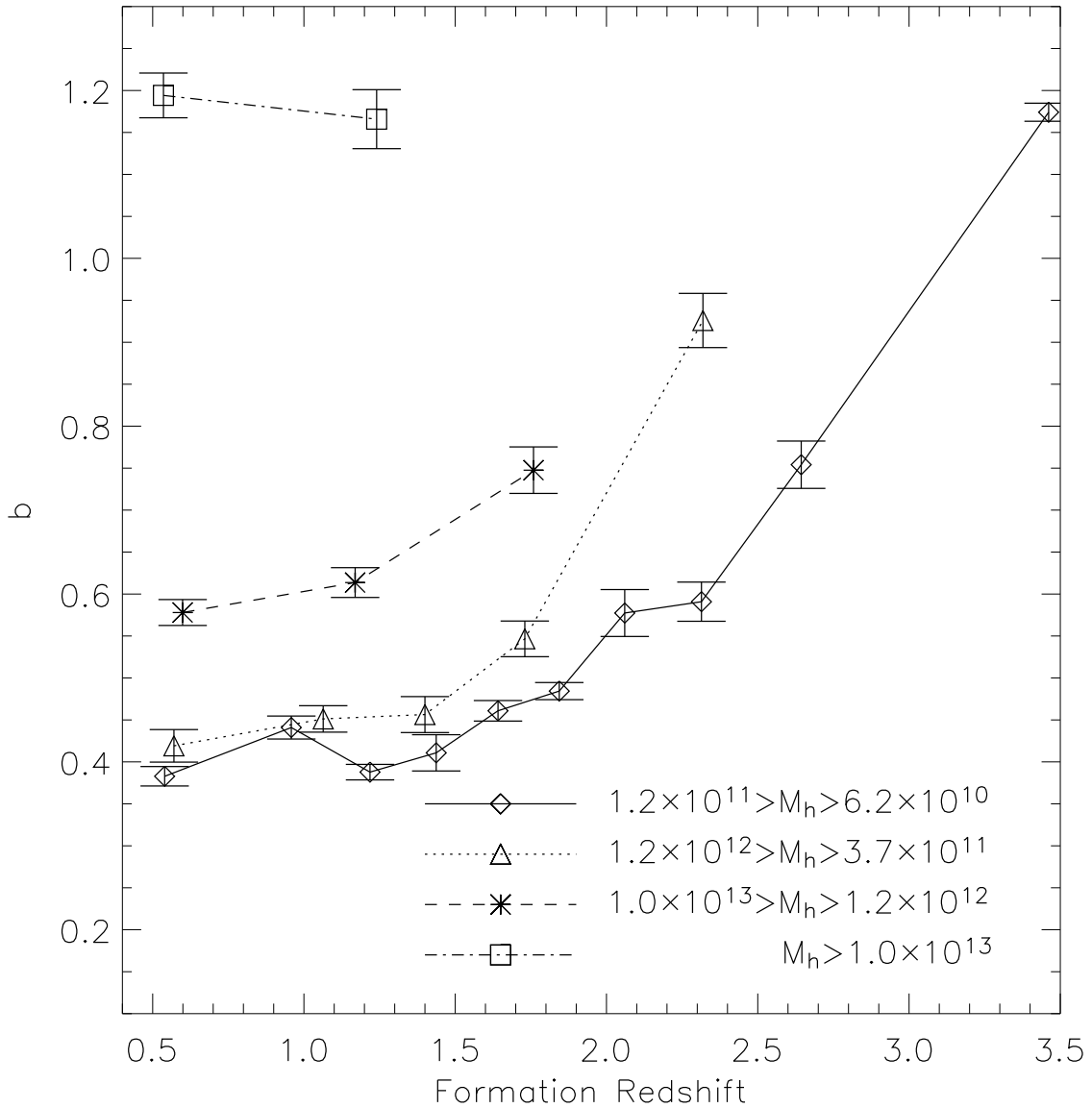


Figure 2. The bias factor, defined by Eq. 1, as a function of halo formation redshift. Results are shown for halos in different mass ranges, as indicated in the panel.

in consideration will eventually end up should be equal to M_i instead of M_{i1} . The reason for this is discussed in detail in Sheth, Mo & Tormen (2001). In Figs.3 we show the ratio between the initial mass M_i and the final halo mass, M_h , versus halo formation time for halos in two mass ranges. These plots show that, for many low-mass halos, the initial mass assigned according to the spherical collapse model is much larger than the final halo mass. Note that the initial/final mass ratio can be as large as 1,000 for some low-mass halos. This discrepancy between the Press-Schechter theory and cosmological simulations has been discussed in considerable detail in Sheth et al. (2001), and is the primary reason why Press-

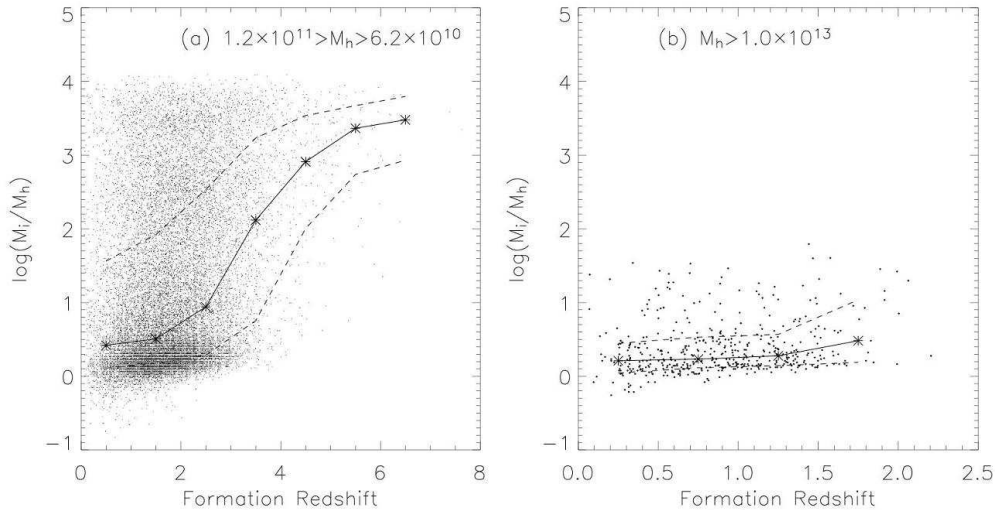


Figure 3. The ratio between initial mass, M_i , and the final mass M_h as a function of halo formation redshift. Left panel is for low-mass halos with $1.2 \times 10^{11} h^{-1} M_\odot > M_h > 6.2 \times 10^{10} h^{-1} M_\odot$, while right panel is for halos with $M_h > 1.0 \times 10^{13} h^{-1} M_\odot$. The three curves in each panel represent the median, 20 and 80 percentiles.

Schechter formula over-predicts the abundance of low-mass halos. For high-mass halos, the ratios are much closer to 1, suggesting that Press-Schechter formalism works better for high-mass halos.

Fig. 3 also shows a clear trend that the initial/final mass ratio on average increases with the formation redshift, and the trend is stronger for halos of lower masses. According to the halo bias model of Mo & White (1996), which is based on identifying halos in the initial density field according to spherical collapse model, halos of larger masses should be more strongly correlated. It is therefore interesting to check whether the age-dependence of halo clustering observed in the simulation can be explained by the correlation between initial mass and formation time obtained here. To do this, we select low-mass halos with final masses $1.2 \times 10^{11} h^{-1} M_\odot > M_h > 6.2 \times 10^{10} h^{-1} M_\odot$, and massive halos with final masses $M_h > 10^{13} h^{-1} M_\odot$. We bin halos in each of the two mass ranges according to their initial masses M_i , and compute the bias factor as a function of M_i . The results are shown in Fig. 4. As expected, the bias factor increases strongly with mass. The prediction of the Mo & White (1996) bias model is shown as the solid curve. The model matches the simulation result for $M_i \gg M_*$, suggesting that large spherical patches are strongly clustered regardless of whether or not a small halo will eventually form in them. However, for $M_i \lesssim M_*$, the model overpredicts the bias factor. This is not surprising, because small patches in which a low-mass halo form at the present time are biased towards low-density regions.

We can assign to each halo a bias factor, b , according to its initial mass M_i using the bias-mass relation given by the simulation. We can then average the values of b for halos in bins

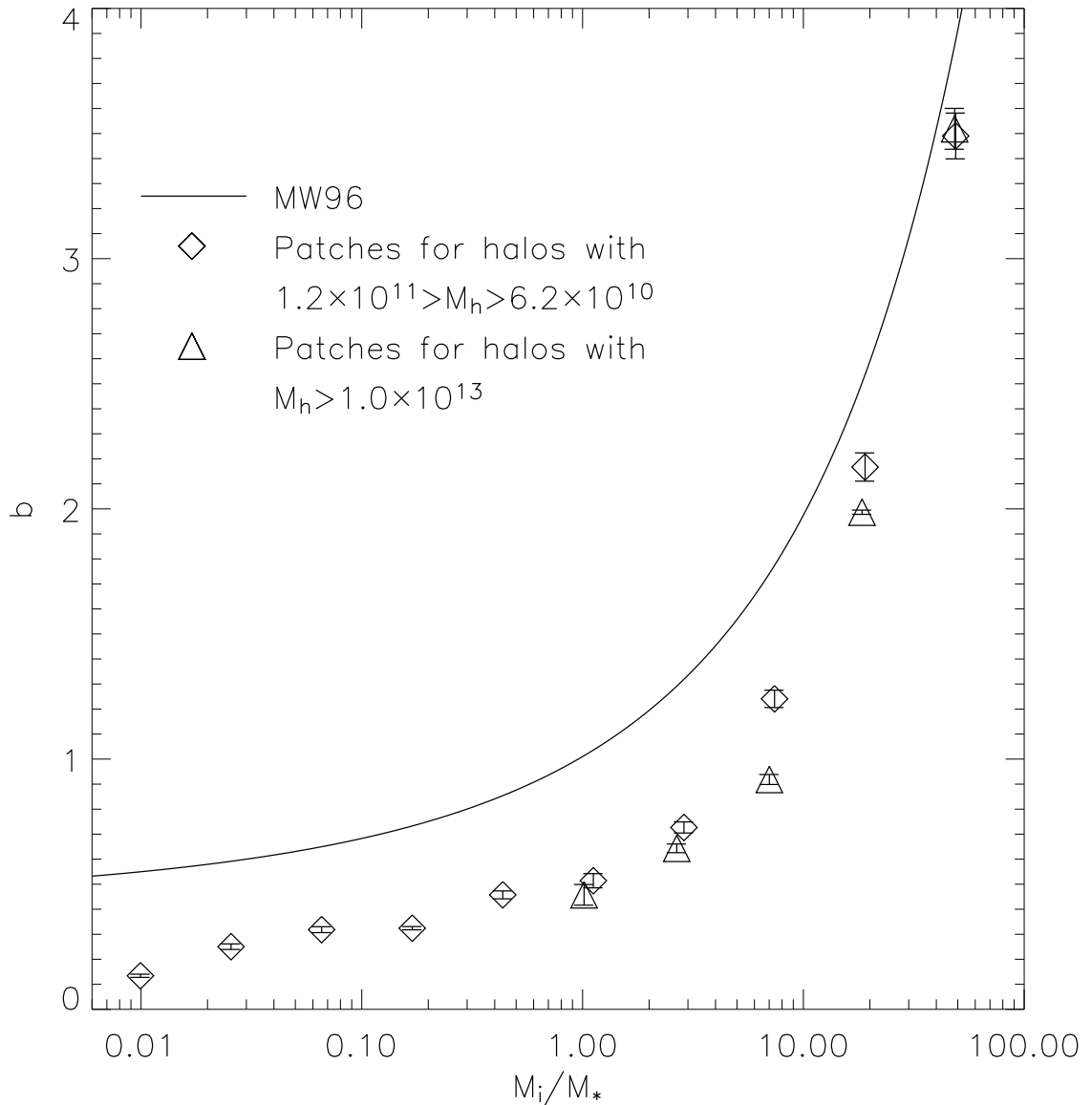


Figure 4. Bias factor as a function of initial mass M_i for low-mass halos with $1.2 \times 10^{11} h^{-1} M_\odot > M_h > 6.2 \times 10^{10} h^{-1} M_\odot$ (squares), and massive halos with $M_h > 1.0 \times 10^{13} h^{-1} M_\odot$ (triangles). The solid curve shows the prediction of the Mo & White (1996) bias model.

of formation redshift to predict the age-dependence of halo clustering. The dashed curves in Fig. 5 show the bias-formation redshift relations obtained in this way for halos in two mass ranges. The predictions match well the simulation results, suggesting that the observed age-dependence of clustering for halos of a given final mass can be entirely explained by the difference in the initial mass. Old, low-mass halos are more strongly clustered than their younger counterparts simply because they are associated with perturbations of higher mass (i.e. patches corresponding to higher peaks) in the initial density field. The age-dependence is weaker for more massive halos, because their M_i represent their final masses more faithfully.

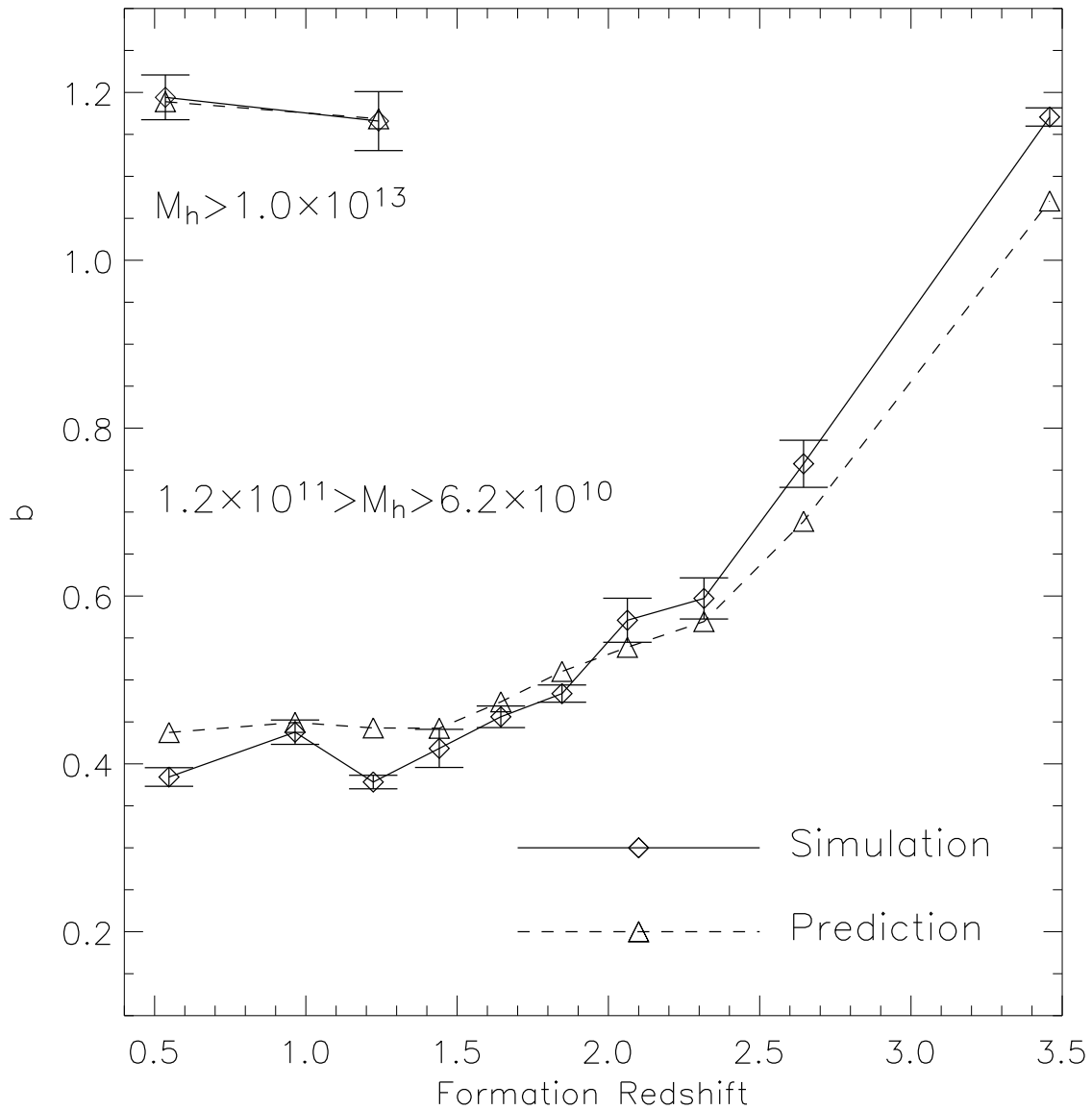


Figure 5. Bias factor as a function of formation redshift. Symbols connected with solid lines are the results obtained from simulations (the same as those shown in Fig. 2), while symbols connected by dashed lines are the corresponding predictions based on the correlation between bias and initial mass (see text for detail). Results are shown for low-mass halos with $1.2 \times 10^{11} h^{-1} M_\odot > M_h > 6.2 \times 10^{10} h^{-1} M_\odot$, and for massive halos with $M_h > 1.0 \times 10^{13} h^{-1} M_\odot$, as indicated in the panel. For the other two mass ranges shown in Fig 2, the model predictions match the simulation results as well. They are not plotted here for the sake of clarity.

4 THE ENVIRONMENTAL EFFECTS OF HALO FORMATION

The question is, of course, why some low-mass halos can survive in a patch which itself should collapse to form a virialized halo according to spherical collapse model, and what prevents such halos from accreting mass in later times. To have some ideas about what is going on during the formation of a low-mass old halo, we show in Fig. 6 the spatial distribution of dark matter particles in the neighborhood of such a halo for a number of representative

snapshots, with the particles that eventually end up in the final halo marked in colour. As one can see, the main part of the small halo collapses quickly to form a halo, which then grows only slowly while orbiting around a bigger halo that forms later. The early collapse is driven largely by the relatively high initial density of the material associated with the halo, as is demonstrated in Fig. 7 which shows the initial overdensity around a halo center as a function of halo formation redshift. In Fig. 7 the overdensity is defined as the mean within a sphere that is centered at the initial position of the halo and has a radius such that the total mass it contains is equal to the mass of the halo. For low-mass halos, there is a strong, positive correlation between the mean overdensity and the formation time. Halos with earlier formation times have initial overdensity much higher than the critical density for spherical collapse (indicated as the horizontal line in the figure). With such overdensities, these perturbations can collapse in early times to form virialized halos. The situation is very different for massive halos, where the mean overdensity are all close to the critical value for spherical collapse [see Fig. 7(b)].

There are two possibilities why low-mass old halos stop accreting mass at relatively early times. The first is that these halos reside in locally low-density regions, and so there is no material for them to accrete. To test this, we estimate the total mass between r_{vir} and $3r_{\text{vir}}$ (with r_{vir} the virial radius) for each halo and plot the mean mass density (in units of mean density of the universe) within these two radii versus halo formation redshift in Fig. 8(a). This figure shows that there is in fact a slightly larger amount of mass around older halos, and so the truncation of the growth of old, low-mass halos cannot be explained by the lack of material around them. However, the availability of material is a necessary, not a sufficient condition for halo accretion. In order for the material around a halo to be accreted by the halo, the velocity of the material to be accreted relative to the halo must be sufficiently low. To see if this condition is fulfilled, we estimate the velocity difference $|\mathbf{v}_p - \mathbf{v}_h|$ for all particles with halo-centric distances between r_{vir} and $3r_{\text{vir}}$, where \mathbf{v}_h is the velocity of the host halo, and \mathbf{v}_p is the velocity of a CDM particle. Fig. 8(b) shows the velocity difference (in units of halo virial velocity) versus halo formation redshift. There is a clear trend that particles in the neighborhood of an older halo have systematically larger velocity differences with the host halo. For the oldest halos, the velocity differences for most particles are significantly larger than the virial velocities of the halos. These particles cannot be accreted by the halo, because they are too energetic. Thus, the reason why late accretions by old, low-mass halos are truncated is that they are embedded in ‘hot’ regions where particles are moving too

fast for them to capture. The situation is very different for massive halos [Figs. 8(c) and (d)]. First of all, the mean densities in their neighborhoods are quite independent of halo formation redshift [Fig. 8(c)]. More importantly, the velocity differences between a halo and particles around it are smaller than the virial velocity and so most of these particles can be accreted by the halo in subsequent evolution.

It is easy to understand why old, low-mass halos are embedded in hot environments. As shown in Fig. 6, these halos are formed in the vicinity of big structures that are dominated by one or more massive halos. To see this more clearly, we plot in Fig. 9 the mass of the most massive neighboring halo within a distance of $2h^{-1}\text{Mpc}$ from a low-mass halo as a function of the formation redshift of the low-mass halo. An old low-mass halo almost always has a massive halo in its neighborhood. These old low-mass halos are similar to the subhalo population seen in high-resolution N -body simulations (e.g. Klypin et al. 1999; Moore et al. 1999), except that they have not yet merged into the virialized part of a massive halo. Although the formation of the more massive neighboring halos occurred at later times, the tidal field of the large structure can accelerate the particles around low-mass halos, thereby increasing their velocities relative to the low-mass halos. Furthermore, massive pancakes and filaments can form in high-density patches prior to the formation of massive halos, and heat up the particles in them in a way similar to the preheating mechanism discussed in Mo et al. (2005). Note that these two processes are related, because the formation of pancakes and filaments is related to the local tidal field. As discussed in Mo et al. (2005), the tidal effect and preheating are expected to have more significant impact on smaller halos, which may explain why the age-dependence of halo clustering is weaker for more massive halos.

5 DISCUSSION AND SUMMARY

In this paper, we have used a high-resolution N -body simulation to study how the formation of CDM halos may be affected by their environments, and how such environmental effects may produce the age-dependence of halo clustering seen in recent large N -body simulations. We have shown that old low-mass halos are almost always associated with initial perturbations that correspond to higher peaks than their present masses imply. Consequently, these halos are strongly clustered in space despite of their low masses at the present time. Because of their associations with large density perturbations, old low-mass halos are almost always found in the vicinity of big structures that are dominated by one or more massive halos at

the present time. Mass accretions into these low-mass halos are limited at late times by the tidal field of the larger neighboring structures. Such environmental effects are weaker for more massive halos, which explains why the age-dependence of halo clustering is weaker for more massive halos.

Our results demonstrate clearly that environmental effects play an important role during the formation of dark matter halos, especially of low-mass halos. Since the properties of galaxies that form in a halo are expected to depend on the formation history of the halo, such environmental effects may have important implications for galaxy formation in different environments. Galaxies that form in old, low-mass halos are presumably old and faint, and our results suggest that many such galaxies may be located in the vicinity of relatively massive galaxy systems. These galaxies likely represent an extension of the satellite galaxies observed in galaxy systems such as the local group and other groups/clusters of galaxies. Observationally, it is known that satellite galaxies in galaxy groups are dynamically old systems (dwarf ellipticals and dwarf spheroids) that contain mainly old stellar populations. It is interesting to see whether the stellar populations and kinematics of low-mass galaxies in the neighborhoods of nearby galaxy groups have properties similar to those of the satellite population.

Theoretically, it is very interesting to see if the ellipsoidal collapse model that incorporates large-scale tidal field into the dynamics can indeed explain the environmental effects discussed here and the age-dependence of halo clustering observed in N -body simulations. We will come back to this problem in a future work.

ACKNOWLEDGMENT

We thank Xi Kang and Guangtun Zhu for help in constructing merger trees from the simulation, Adrian Jenkins, the referee of the paper, for helpful comments. HJM would like to acknowledge the support of NSF AST-0607535, NASA AISR-126270 and NSF IIS-0611948. YPJ is supported by the grants from NSFC (No. 10373012, 10533030) and from Shanghai Key Projects in Basic research (No. 04JC14079 and 05XD14019). HYW and HJM acknowledge supports from the Chinese Academy of Sciences for the visit at Shanghai Astronomical Observatory.

REFERENCES

- Bardeen J. M., Bond J. R., Kaiser N., Szalay A. S., 1986, *ApJ*, 304, 15
- Bond J. R., Cole S., Efstathiou G., Kaiser N., 1991, *ApJ*, 379, 440
- Davis M., Efstathiou G., Frenk C. S., White S. D. M., 1985, *ApJ*, 292, 371
- Gao L., Springel V., White S. D. M., 2005, *MNRAS*, 363, L66
- Harker G., Cole S., Helly J., Frenk C., Jenkins A., 2006, *MNRAS*, 367, 1039
- Jing Y. P., 1998, *ApJ*, 503, L9
- Jing, Y. P. 2000, *ApJ*, 535, 30
- Jing Y.P., Mo H.J., Börner G., 1998, *ApJ*, 494, 1
- Jing Y. P., Suto Y., 2002, *ApJ*, 574, 538
- Jing Y.P., Suto Y., 2000, *ApJ*, 529L, 69
- Klypin A. Gottlöber S., Kravtsov A.V., Khokhlov A.M., 1999, *ApJ*, 516, 530
- Li Y., Mo H. J., van den Bosch F. C., 2005, preprint, arXiv:astro-ph/0510372
- Lu Y., Mo H. J., Katz N., Weinberg M. D., 2006, *MNRAS*, 368, 1931
- Ma C.-P., Fry J. N., 2000, *ApJ*, 543, 503
- Mo H. J., Jing Y. P., Börner G., 1997, *MNRAS*, 286, 979
- Mo H. J., White S. D. M., 1996, *MNRAS*, 282, 347
- Mo H. J., Yang X., van den Bosch F. C., Katz N., 2005, *MNRAS*, 363, 1155
- Moore B., Ghigna S., Governato G., Lake G., Quinn T., Stadel J., Tozzi P., 1999, *ApJ*, 524, L19
- Navarro J. F., Frenk C. S., White S. D. M., 1997, *ApJ*, 490, 493
- Peacock J. A., Smith R. E., 2000, *MNRAS*, 318, 1144
- Press W. H., Schechter P., 1974, *ApJ*, 187, 425
- Seljak U., 2000, *MNRAS*, 318, 203
- Seljak U., Warren M. S., 2004, *MNRAS*, 355, 129
- Sheth R. K., Mo H. J., Tormen G., 2001, *MNRAS*, 323, 1
- Wechsler R. H., Bullock J. S., Primack J. R., Kravtsov A. V., Dekel A., 2002, *ApJ*, 568, 52
- Wechsler R. H., Zentner A. R., Bullock J. S., Kravtsov A. V., Allgood B., 2005, preprint, arXiv:astro-ph/0512416
- Wetzel A. R., Cohn J. D., White M., Holz D. E., Warren M. S., 2006, preprint, arXiv:astro-ph/0606699
- Yang X., Mo H. J., van den Bosch F. C., 2003, *MNRAS*, 339, 1057

Zhao D. H., Jing Y. P., Mo H. J., Börner G., 2003, ApJ, 597, L9

Zhao D. H., Mo H. J., Jing Y. P., Börner G., 2003, MNRAS, 339, 12

Zheng Z., et al., 2005, ApJ, 633, 791

Zhu G., Zheng Z., Lin W. P., Jing Y. P., Kang X., Gao L., 2006, ApJ, 639, L5

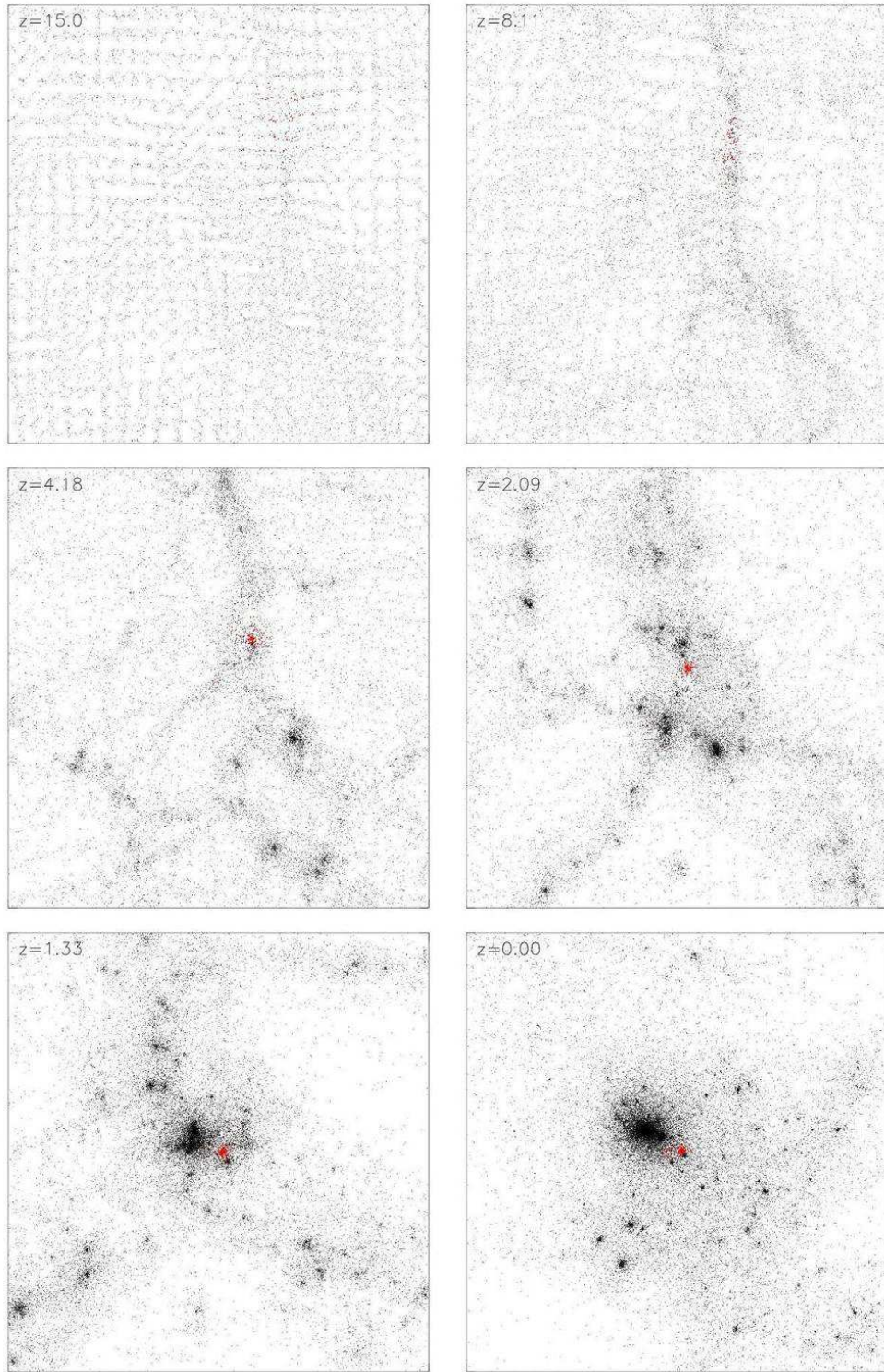


Figure 6. CDM particle distributions around a low-mass old halo (with final mass $M_h = 1.2 \times 10^{11} h^{-1} M_\odot$ and formation redshift 3.86) at a number of different redshifts (as indicated in the panels). Particles that eventually end up in the final halo are plotted in red.

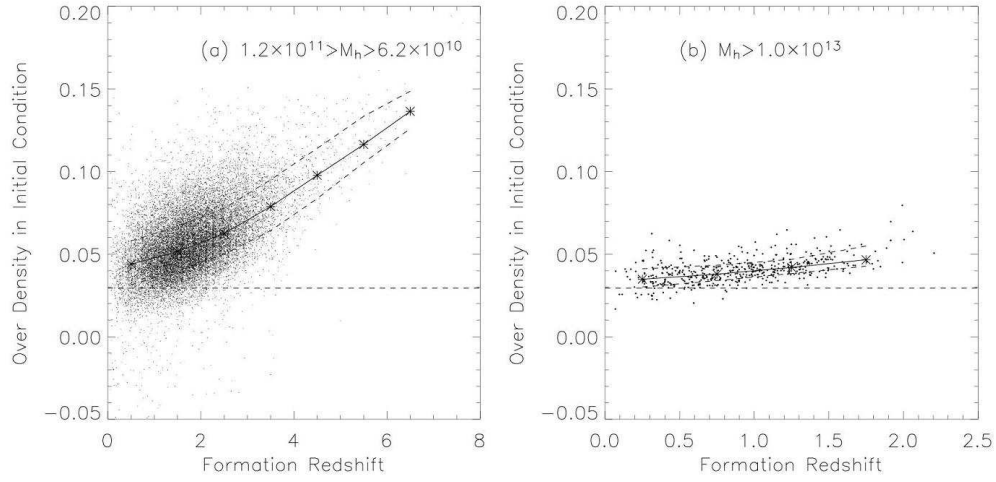


Figure 7. The correlation between the initial overdensity, defined on the halo mass scale, and halo formation redshift. Results are shown for low-mass halos with $1.2 \times 10^{11} h^{-1} M_{\odot} > M_h > 6.2 \times 10^{10} h^{-1} M_{\odot}$ (left panel) and for massive halos with $M_h > 1.0 \times 10^{13} h^{-1} M_{\odot}$ (right panel). The three curves in each panel show the median, 20 and 80 percentiles. The horizontal lines indicates the critical overdensity for collapse (at the initial redshift $z = 72$) based on spherical collapse model.

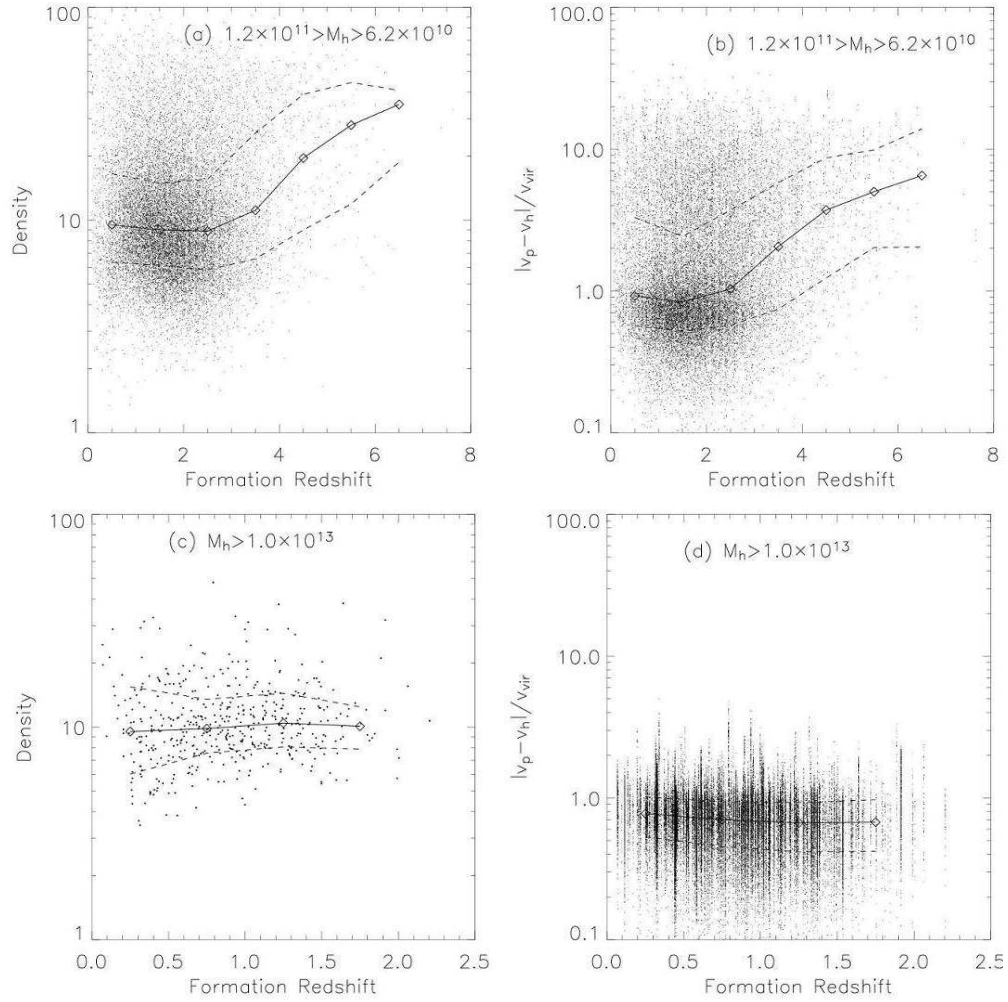


Figure 8. Left panels: the mean density (in units of the mean density of the universe) between r_{vir} and $3r_{vir}$ as a function of halo formation redshift. Each point represents a halo. Right panels: the velocity difference for particles located between r_{vir} and $3r_{vir}$ as a function of halo formation redshift. Here each point represents a dark matter particle. Upper panels are for low-mass halos with $1.2 \times 10^{11} h^{-1} M_{\odot} > M_h > 6.2 \times 10^{10} h^{-1} M_{\odot}$, and lower panels are for massive halos with $M_h > 1.0 \times 10^{13} h^{-1} M_{\odot}$. The three curves in each panel are the median, 20 and 80 percentiles.

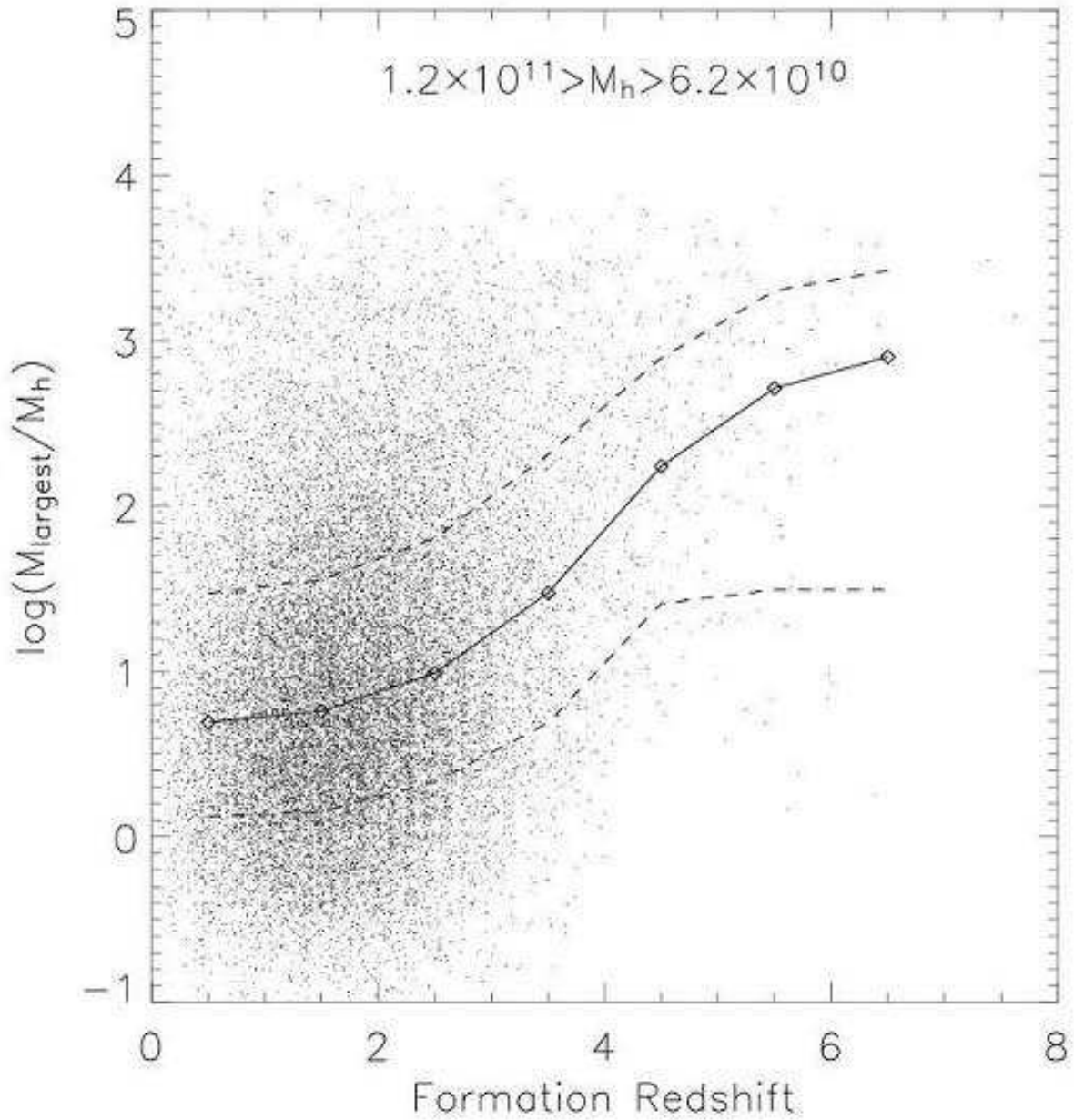


Figure 9. The ratio between M_{largest} and M_h as a function of halo formation redshift. Here M_{largest} is defined to be the mass of the most massive halo that is within $2h^{-1}\text{Mpc}$ from the halo in consideration. The three curves show the median, 20 and 80 percentiles.